Advances in Aircraft and Spacecraft Science, *Vol. 2, No. 3 (2015) 345-365*
DOI: http://dx.doi.org/10.12989/aas.2015.2.3.345

A load-bearing structural element with energy dissipation capability under harmonic excitation

Michael E. Pontecorvo[1], Silvestro Barbarino[1], Farhan S. Gandhi[*1], Scott Bland[2], Robert Snyder[2], Jay Kudva[2] and Edward V. White[3]

[1]*Rensselaer Polytechnic Institute, Troy, NY, 12180, USA*
[2]*NextGen Aeronautics Inc., Torrance, CA, 90505, USA*
[3]*The Boeing Company, Berkeley, MO, 63134, USA*

(Received May 8, 2014, Revised June 26, 2014, Accepted July 9, 2014)

Abstract. This paper focuses on the design, fabrication, testing and analysis of a novel load-bearing element with energy dissipation capability. A single element comprises two von-Mises trusses (VMTs), which are sandwiched between two plates and connected to dashpots that stroke as the VMTs cycle between stable equilibrium states. The elements can be assembled in-plane to form a large plate-like structure or stacked with different properties in each layer for improved load-adaptability. Also introduced in the elements are pre-loaded springs (PLSs) that provide high initial stiffness and allow the element to carry a static load even when the VMTs cannot under harmonic disturbance input. Simulations of the system behavior using the Simscape environment show good overall correlation with test data. Good energy dissipation capability is observed over a frequency range from 0.1 Hz to 2 Hz. The test and simulation results show that a two layer prototype, having one soft VMT layer and one stiff VMT layer, can provide good energy dissipation over a decade of variation in harmonic load amplitude, while retaining the ability to carry static load due to the PLSs. The paper discusses how system design parameter changes affect the static load capability and the hysteresis behavior.

Keywords: load adaptability; damping; energy dissipation; von-Mises truss; snap-through

1. Introduction

Structural elements that can simultaneously bear load and provide energy dissipation capability under disturbance are of great interest in many aerospace, mechanical and civil engineering applications. This paper presents a novel, sandwiched-plate-like structural element that supports loads up to a designed limit, beyond which internal von-Mises truss (VMT) mechanisms snap-through and facilitate energy dissipation. The structural element can be layered to improve dissipation capability over a wide range of disturbance load amplitudes. This work builds on a previous study by Barbarino *et al*. (2012) which uses the von-Mises truss as an energy dissipation mechanism. Introduced by Mises (1923), the von-Mises truss is composed of two rigid links, pinned together at the vertex, whose endpoints are spring-restrained and constrained to move along a line perpendicular to the motion of the vertex. VMTs exhibit a nonlinear force-deflection curve

*Corresponding author, Professor, E-mail: gandhf@rpi.edu

http://www.techno-press.org/?journal=aas&subpage=7 ISSN: 2287-528X (Print), 2287-5271 (Online)

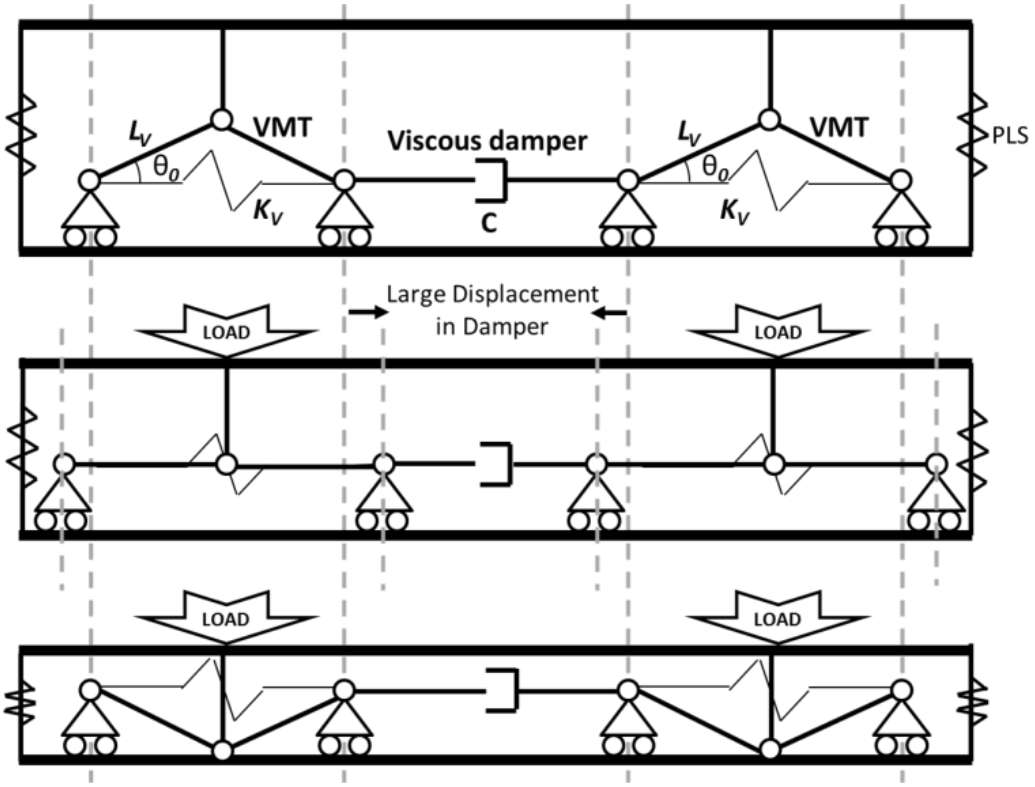

Fig. 1 Diagram of the proposed structural configuration

that contains one unstable and two stable equilibrium positions. When a VMT is forced away from one stable equilibrium position, energy is first stored in the system. On passing through the unstable equilibrium position, the stored energy is released, and the VMT rapidly moves to the second stable equilibrium position. This phenomenon is known as snap-through. Several researchers have considered the dynamic behavior of a VMT system. Blair *et al*. (1992) investigated trusses under harmonic forcing, Avramov and Mikhlin (2006) considered the use of the truss as a vibration absorber, Kounadis *et al*. (1989) studied the truss under impact loading, Padthe *et al*. (2008) presented the hysteretic behavior of the truss, and Murray and Gandhi (2011) examined the effect of damping on reducing the transient oscillation associated with snap-through. Continuous analogs of the VMT, such as elastic arches (Johnson *et al*. 2010, Timoshenko 1936), bi-stable composite plates (Diaconu *et al*. 2007), and other bi-stable compliant devices (Howell 2001, Jensen *et al*. 2001, Jensen and Howell 2004) have also been widely studied for use as switches and morphing mechanisms.

Barbarino *et al*. (2012) presented computational results showing that the high velocity of the VMT vertex during snap-through, connected to a damping element, can result in very large system loss factor values (in excess of 0.6). The present study significantly expands on the idea presented in the numerical study by Barbarino *et al*. (2012) in the following specific areas: (1) the design and fabrication of a sandwiched-plate-like structural element with VMTs and dashpots integrated between the face-plates; (2) extension to multiple stacked layers for improved performance under disturbance load amplitude variation; (3) introduction of a pre-loaded spring (PLS) in parallel with

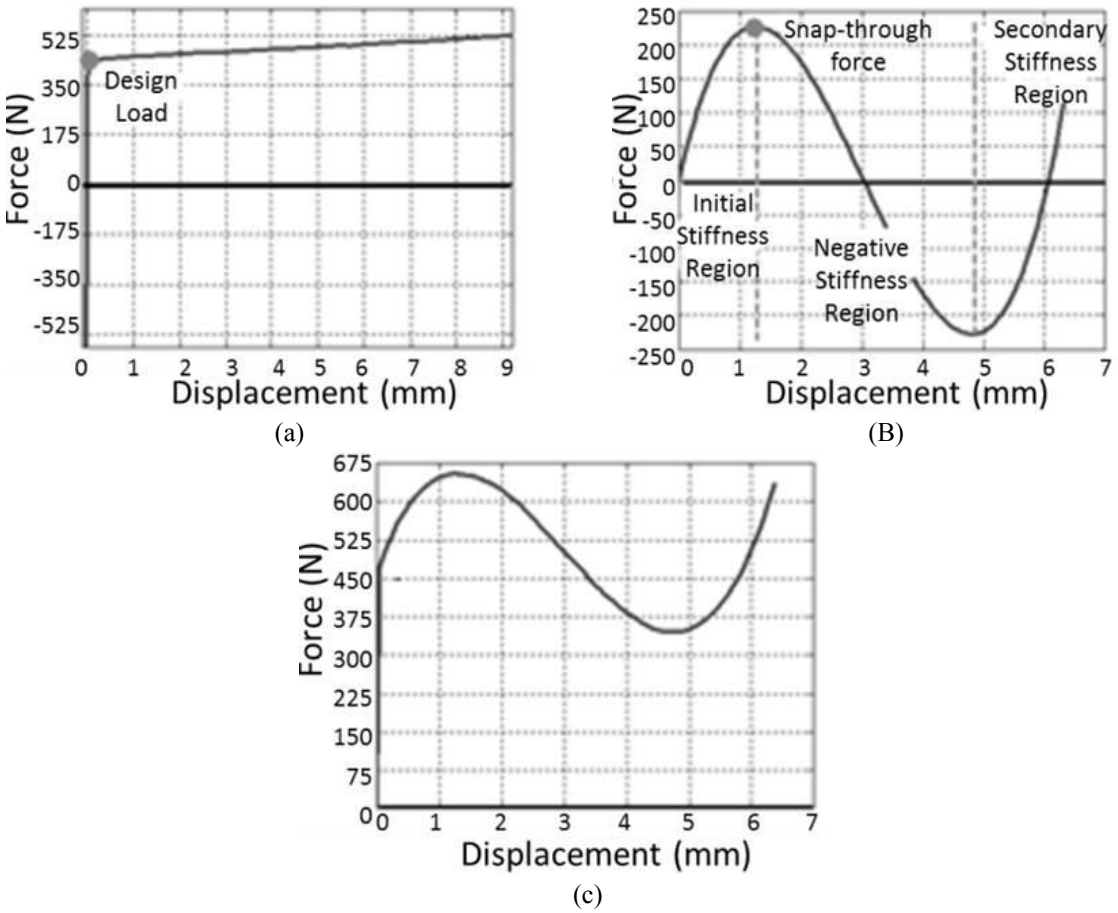

Fig. 2 Quasi-static behavior of (a) the bi-linear spring, (b) the VMT, and (c) the combined system

the VMT to provide high static load-carrying capability; and (4) validation of simulation results with prototype test results under harmonic displacement input.

2. Conceptual design

Integration of the VMT, viscous dampers, and PLS was envisioned in a compact sandwiched-plate-like element. Fig. 1 represents a schematic sketch of the proposed configuration and its operation. The element shows two VMTs sandwiched between two rigid plates and is designed to be loaded along the thickness direction. By connecting the viscous damper to the base of the VMT links, as shown, the dashpot contracts as the VMT moves from the first stable equilibrium position (top figure) to the unstable equilibrium position (middle figure), and then expands again as the VMT moves to the second stable equilibrium position (bottom figure). This configuration, featuring orthogonal VMT vertex and dashpot motion, is highly compact and space-efficient. It is interesting to note that as the VMT undergoes a half-cycle of motion (from the top to the bottom in Fig. 1), the viscous damper has gone through a full cycle of motion. Thus, if the plate and VMT

vertex is subjected to a harmonic displacement, the dashpot motion is at twice that frequency. Note that the design presented in Fig. 1 is essentially a single "tile" and many such tiles can be assembled in-plane to form a large panel. Viscous dampers would connect from the VMTs shown in Fig. 1 to the VMTs in the adjacent tiles, and the rigid faceplates could be contiguous across tiles, to form a highly integrated panel structure.

The static force/displacement behavior of a VMT alone is depicted in Fig. 2(b). It is seen that the VMT alone can carry a maximum load (denoted on the figure as snap-through force), but it loses this load carrying capability during transition from one stable equilibrium state to the next. The goal is to develop an element that has relatively high design load carrying capability and static stiffness (low displacement under design static load), and yet can undergo large deformation and display good energy dissipation under disturbance while continuing to carry the design static load. Introduction of a bi-linear spring (Fig. 2(a)) in parallel to the VMT results in the force/displacement behavior depicted in Fig. 2(c). Note that the design load is still carried in Fig. 2(c), even as the VMT snaps-through under a superposed disturbance. The inflection point, or critical load, of the bi-linear spring can be matched to the static (design) load for the application. The VMT geometry and spring stiffness (K_v), on the other hand, can be selected to achieve a desired snap-through force which can be matched to the amplitude of expected disturbance loads.

A bi-linear spring with high initial stiffness, and reduced stiffness beyond a critical load, can be realized in a number of ways. One approach could be to use a buckling beam. Another approach, adopted in the current study, is to use pre-loaded springs (PLSs), which are shown in Fig. 1 surrounding telescoping guide-rods. The springs are pre-loaded by compressing them down and placing them between the upper and lower plates. Due to the rigid connection between the top plate and the VMT vertex, the compression in the spring cannot be released as it would cause the bases of the VMT elements to come together and this is prevented by mechanical stops. The PLS is a fairly compliant spring and a high preload is achieved by putting the spring through a large pre-strain, rather than using a high spring-rate. A compliant PLS allows the dynamic response under a harmonic excitation to be dominated largely by the VMT and not significantly affected by the PLS. If the pre-loaded spring were very stiff relative to the VMT spring, this could suppress the snap-through behavior. In this combined configuration the PLS can be tailored to achieve the desired initial static load-carrying capability. The von-Mises truss geometry and spring-stiffness can be selected based on desired dashpot stroke and harmonic disturbance load amplitude to maximize energy dissipation.

3. Analysis

In the present study, the Matlab-compatible modeling environment Simscape is used to examine the static and dynamic force/displacement behavior of the structural element. Previous studies in the lead author's group (Barbarino *et al*. 2012, Murray and Gandhi 2011) used Hamilton's principle to derive the governing ODE of the VMT coupled with a dashpot, and numerically integrated this ODE. Simscape uses building blocks that model fundamental mechanical functions and these can be assembled to simulate physical systems. This building-block approach allows the study of larger, more complex systems, and avoids the need to re-derive governing ODEs when experimenting with configuration changes. Blocks representing each component (e.g., beams, springs, dashpots, etc.) are connected to each other and suitable boundary conditions and inputs are applied. The Simscape model of the structural element shown in Fig. 1 is

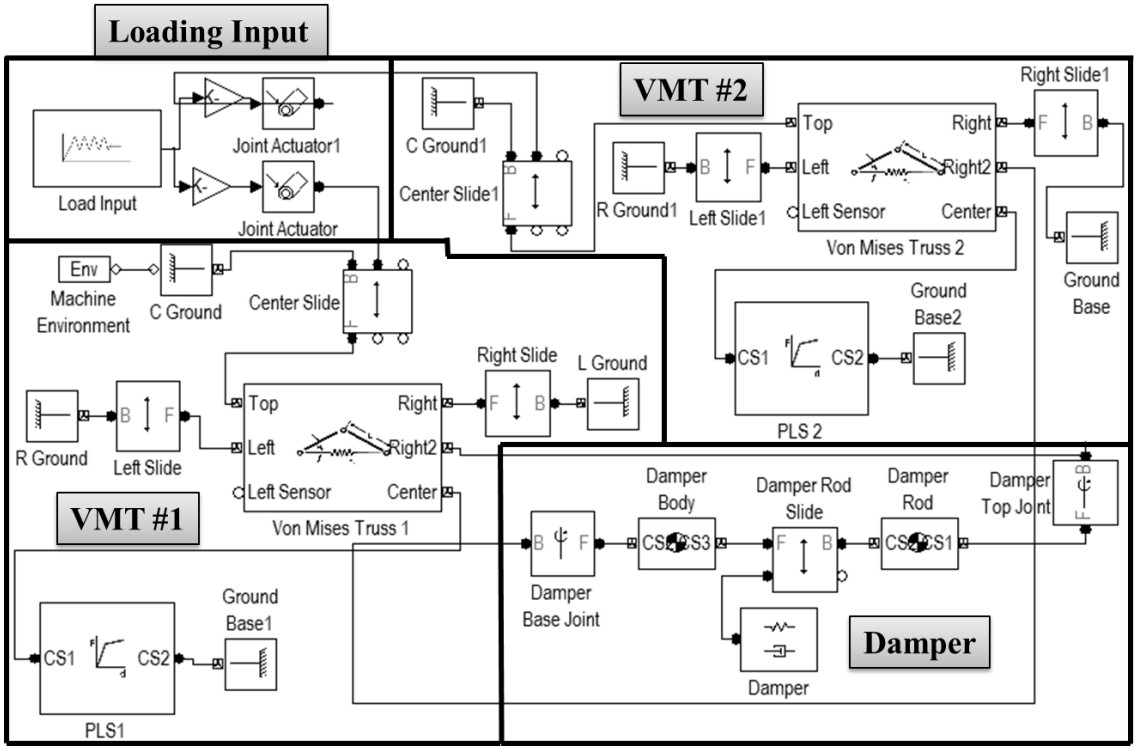

Fig. 3 Simscape block diagram of the schematic in Fig. 1

presented in Fig. 3. The model is composed of four groups: the loading input parameters, the blocks comprising the dashpot, and the two groups of VMT blocks which each contain a block to define the PLS. In Fig. 3, VMT 1 denotes the left VMT in Fig. 1 while VMT 2 denotes the right VMT.

The Simscape model was further expanded to multiple layers (the next section explains the use of multiple layers to adapt to variation in disturbance load amplitude), and fully parameterized to be adjusted to the final design. Fig. 4 presents a schematic of a two layer model in its fully expanded (Fig. 4(a)) and fully compressed (Fig. 4(b)) states. The region highlighted in Fig. 4(b) is representative of the volume which is not subject to variation upon state change, where the dashpots could be located in a prototype. Although not visible in the figures, the PLSs are included in the model.

From the calculated response to a disturbance input by Simscape, force versus displacement hysteresis loops are generated, with the area of the hysteresis representing the dissipative capability of the system (Lazan 1969). The complex modulus method assumes a harmonic response at the same frequency as harmonic excitation and results in an elliptical force/displacement hysteresis loop for linear systems. The force, F, is related to the displacement, x, as follows

$$F = E^{*}x = (E' + jE'')x \tag{1}$$

where E^{*} is the complex modulus comprised of the storage modulus, E' (the real part), and the loss modulus, E'' (the imaginary part). The ratio of the loss modulus to the storage modulus is referred

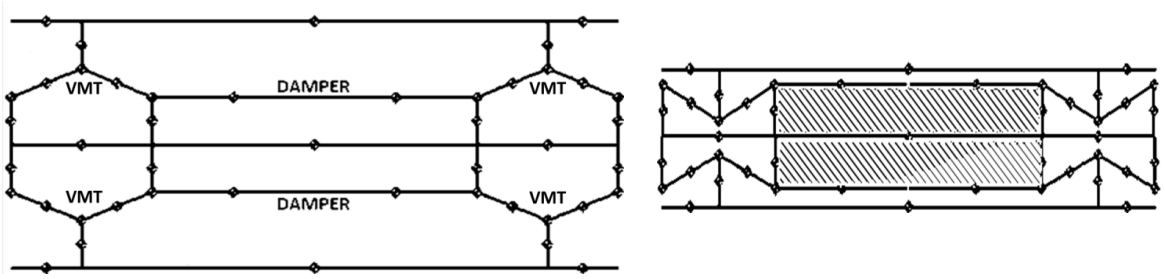

(a) (b)

Fig. 4 Schematic of the two layer model in (a) the fully expanded state and (b) the fully compressed state

to as the loss factor, frequently denoted as tan δ.

$$\tan\delta = \frac{E''}{E'} \tag{2}$$

For nonlinear systems, such as the present system, a harmonic excitation results in a response that would also have higher harmonics, and a non-elliptic force/displacement hysteretic behavior. However, it is noted that the higher harmonics of the response which produce the non-elliptic hysteresis loop shape do not change the loop area, A_{loop}, and hence the energy dissipated (Gandhi and Wolons 1999). Thus A_{loop} is a good damping metric. By filtering out all the higher harmonics of the response and considering only the first harmonic, an equivalent ideal hysteresis loop can be constructed. As an example, assume that the input to the system is a cosine displacement and the response is a vector of force values. The method used in this paper is to take the Fast Fourier Transform of the vector and isolate the fundamental frequency of the response. The magnitude of the fundamental frequency (F_0) and the phase angle (φ_F) are then used to create the ideal elliptical hysteresis loop described by the parametric equations

$$x = x_0\cos(2\pi t) \tag{3}$$

$$F_{ideal} = F_0\cos(2\pi t + \varphi_F) \tag{4}$$

where the input displacement, Eq. (3), is known. The storage and loss moduli are then simply measured from the ideal loop, and the loss factor (tan δ) can be obtained. In the cases where the PLSs are present in the system, the initial stiffness is not considered as part of the hysteresis loop for calculation of tan δ or loop area because no energy is dissipated over this part of the force-displacement curve.

4. Gradient multi-layer design for load adaptability

The Conceptual Design section explained that the VMT could be designed to produce a snap-through force (labeled in Fig. 2(b)) corresponding to the harmonic disturbance force amplitude. However, if the harmonic disturbance force amplitude varies considerably, a stacked multi-layer configuration can be used where the different layers are designed for different snap-through force values. A two layer design, for example, could have a soft layer tuned to a lower snap-through force for low disturbance force amplitude, and a stiff layer tuned to a higher snap-through force for a larger disturbance force amplitude.

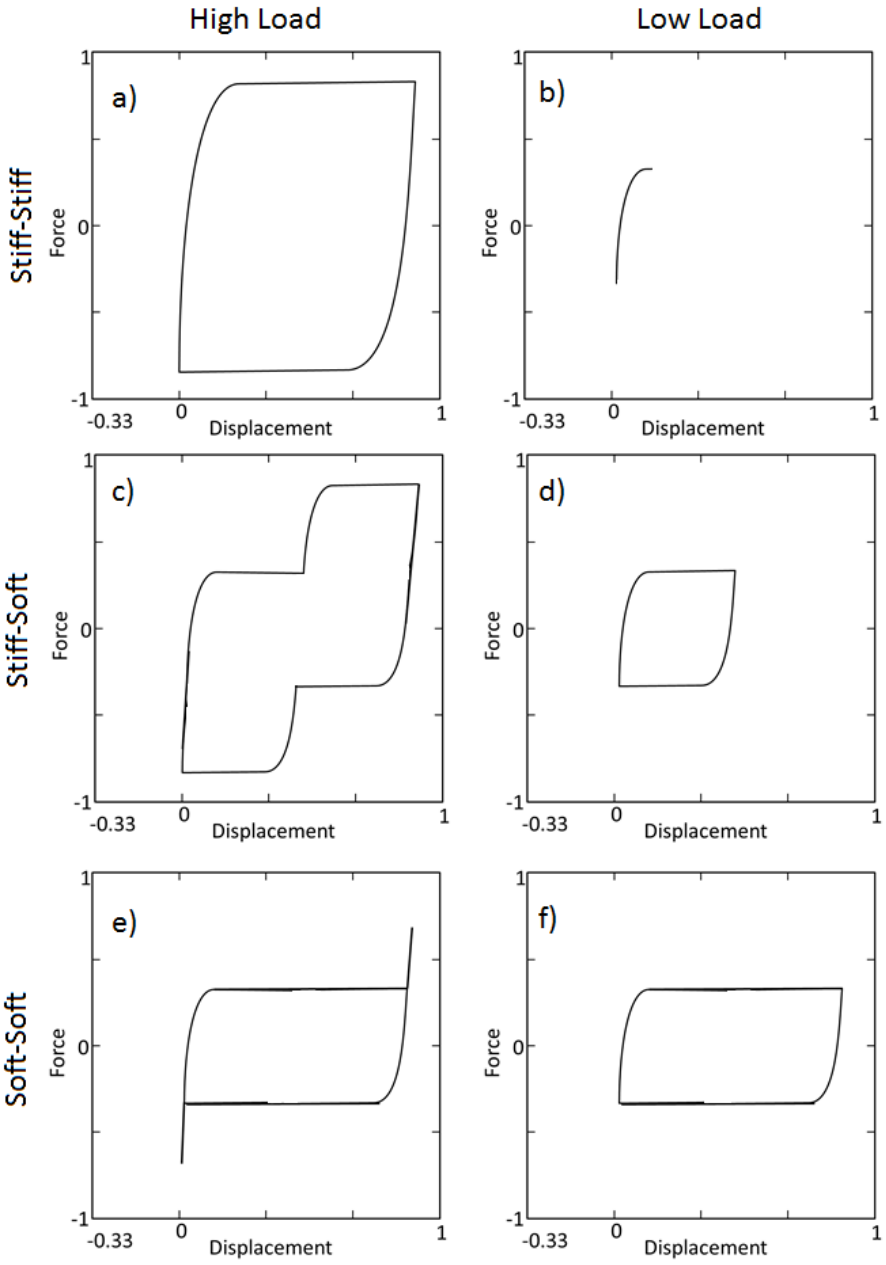

Fig. 5 Simulations of a two layer model under harmonic force input

The advantage of using such a gradient multi-layer design, compared to a system that has only soft layers or only stiff layers, is shown in Fig. 5. Fig. 5(a) shows that under high harmonic force amplitude if both the layers were stiff, the system would dissipate a very large amount of energy, but if the force amplitude reduces, neither layer is able to snap-through and energy dissipation capability is completely lost (Fig. 5(b)). Hysteresis results when both layers are soft are shown in

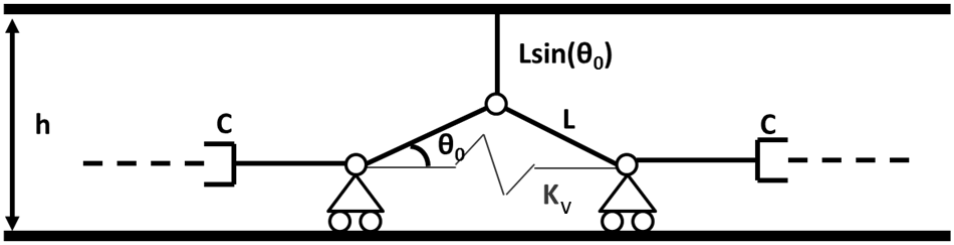

Fig. 6 Prototype design parameters

Figs. 5(e) and 5(f). For low harmonic force amplitude, good energy dissipation is observed in Fig. 5(f), but when the force amplitude increases no increase in energy dissipation is seen in Fig. 5(e), whose performance is substantially inferior to that seen in Fig. 5(a).

By using a soft layer and a stiff layer, a compromise can be achieved. Although the energy dissipation for low harmonic force amplitude (Fig. 5(d)) is less than the maximum seen in Fig. 5(f) since only the softer layer snaps-through, it is certainly an improvement over the stiff-stiff design (Fig. 5(b)). For increased harmonic force amplitude the softer layer snaps through first and then the stiffer layer snaps through (Fig. 5(c)) which produces larger hysteresis area than the soft-soft design (Fig. 5(e)), although the energy dissipation remains less than that seen in the stiff-stiff case (Fig. 5(a)). In other words, while stiff layers are well-suited for high harmonic force amplitude, and soft layers for low force amplitude, a gradient multi-layer design performs reasonably well for both, thus showing good load adaptability characteristics.

5. Prototype design and fabrication

Fig. 6 shows a schematic of part of a single layer with parameters marked on the figure. The parameters of the system are h, the thickness of the layer, c, the viscous damping constant of the dashpots, L, the VMT link length, K_v, the VMT spring constant, and θ_0, the initial angle of the VMT. For compact packaging, requiring the layer to compress as fully as possible, the following geometric constraint applies

$$3Lsin(\theta_0) = h \tag{5}$$

The parameter values were chosen to be h=0.0254 m, c=10 Ns/m, K_v=28,000 N/m, and a concentrated mass of 0.2 kg was placed at the VMT vertex to represent inertia of the links. Using Simscape, a 1 Hz sinusoidal force input with an amplitude just large enough to cause snap-through was applied to the top of the plate.

For increasing values of VMT initial angle, θ_0, and correspondingly decreasing values of L (as per Eq. (5)), Table 1, shows that the total stroke of the dashpot, the work done by the dashpot over a single cycle (same as energy dissipated over a cycle), and the snap-through force, all increase. Since large energy dissipation over a cycle is desirable, nominally, the largest possible initial angle of 60 degrees was chosen.

Next, the components of the schematic in Fig. 6, specifically suitable dashpots, bearings, springs, and sliders for the VMT base, had to be configured. An adjustable viscous damper (Ace Controls Inc. HB15-50-CC-P) was chosen, around which the rest of the system was sized. Pairs of linear bearings from Misumi.com were chosen to allow the horizontal motion of the VMT base

Table 1 Design study results

θ_0 (deg)	L (m)	Total Stroke in Dashpot (m)	Work Done by Dashpot in One Cycle (J)	Snap-Through Force (N)
15	0.0327	0.0022	0.37	12.65
30	0.0169	0.0045	1.72	54.43
45	0.0120	0.0070	4.16	125.65
60	0.0098	0.0098	8.23	246.47

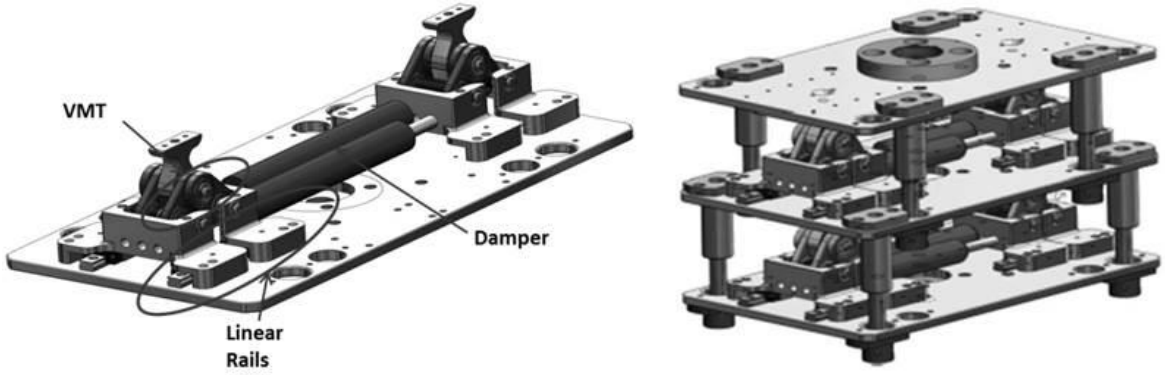

(a) (b)

Fig. 7 CAD model of prototype showing (a) one layer, and (b) two layers stacked

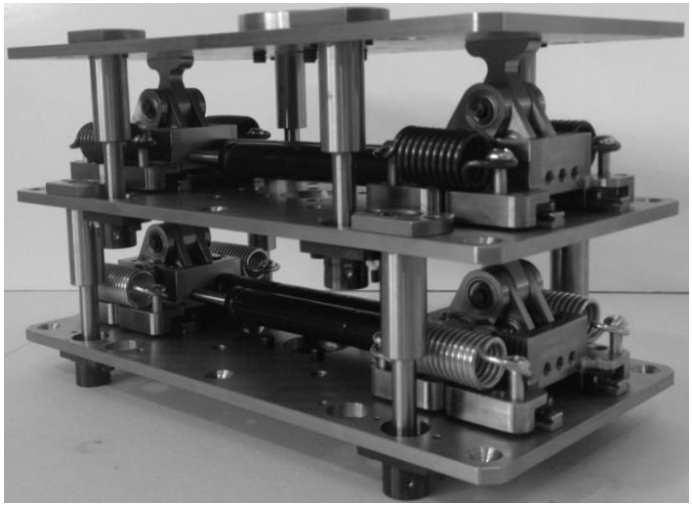

Fig. 8 Complete two layer prototype with 1,068 N/m (top layer) and 4,553 N/m (bottom layer) springs

and small bearings from the same company were chosen for use at the pinned ends of each link. To fit the bearings within the links, the link length had to be extended to 0.015 m. Tension springs ranging in stiffness from 1,068-20,380 N/m were ordered from McMaster-Carr and attached to the sliding bases of the VMTs. Fig. 7(a) shows a CAD model of a single layer of the prototype with the twin dashpots driven by two VMTs on linear rails. Fig. 7(b) shows two layers stacked and

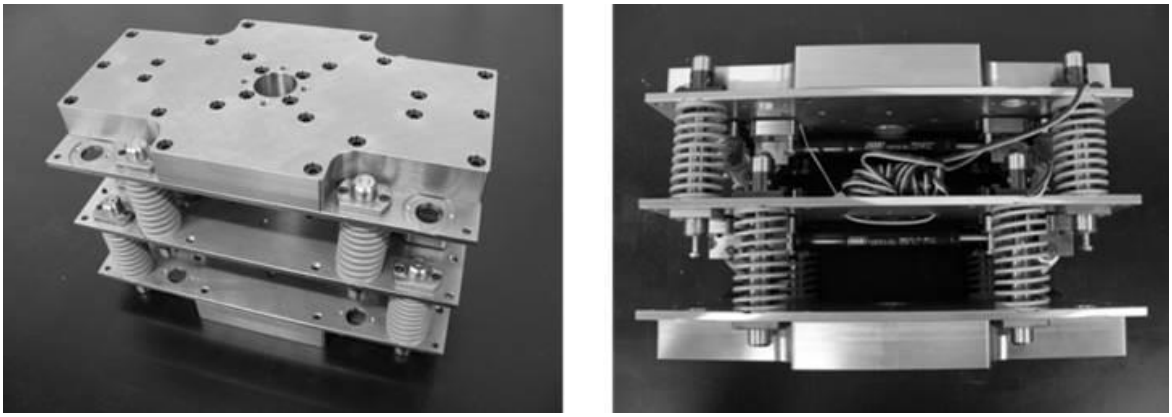

(a) (b)

Fig. 9 Two layer prototype with the 6,200 N/m pre-compressed springs shown in (a) an isometric view and (b) from the side

includes four cylindrical linear guide rails per layer incorporated to prevent the layers from shearing relative to each other.

Fig. 8 shows a photograph of the complete two layer prototype that was fabricated in its fully expanded state. VMT spring stiffness values of 1,068 N/m (top layer) and 4,553 N/m (bottom layer) are used. Each layer is 0.233 m×0.115 m in-plane, has an expanded height of 0.069 m, and can compress 0.027 m to a height of 0.042 m. The maximum expanded height of the layers is slightly limited by the stops on the vertical linear guides, which reduce the initial angle from 60^o to 52^o.

The option of adding four pre-loaded springs (PLSs) to each layer was designed into the prototype. Two different spring stiffnesses were used: 6,200 N/m and 3,080 N/m. Each spring had an initial uncompressed length of 0.1m, and was compressed 0.041 m to fit within a single layer. The pre-compression load in each spring is then the stiffness of the spring multiplied by the pre-compressed length of 0.041 m: 254.2 N for the stiffer springs, and 126.3 N for the softer springs. The design static load of the entire layer is obtained by multiplying the pre-compression load of each spring by the number of springs (four).

Fig. 9 presents two photographs of the two layer prototype with the stiffer PLS installed. During initial tests, it was noticed that the top and bottom plates of the prototype flexed significantly under higher frequency forcing (2-3 Hz) since load is not applied uniformly but only at a central point. In order to stiffen the structure and prevent unwanted bending, two 1” thick steel plates (visible in Fig. 9) were bolted to the top and bottom of the prototype.

6. Single-layer prototype results

The first set of experiments was on a single layer of the prototype with no pre-compressed springs or 1” steel plates. Shown in Fig. 10, the prototype was fixed in a hydraulic MTS 810 machine with the top plate attached to a 13,344 N load cell and the bottom plate attached to the hydraulic piston. A sinusoidal displacement input over the full stroke of the prototype was applied at frequencies from 0.1 to 2 Hz for the cases with no VMT springs, 1,068 N/m springs, and 4,553

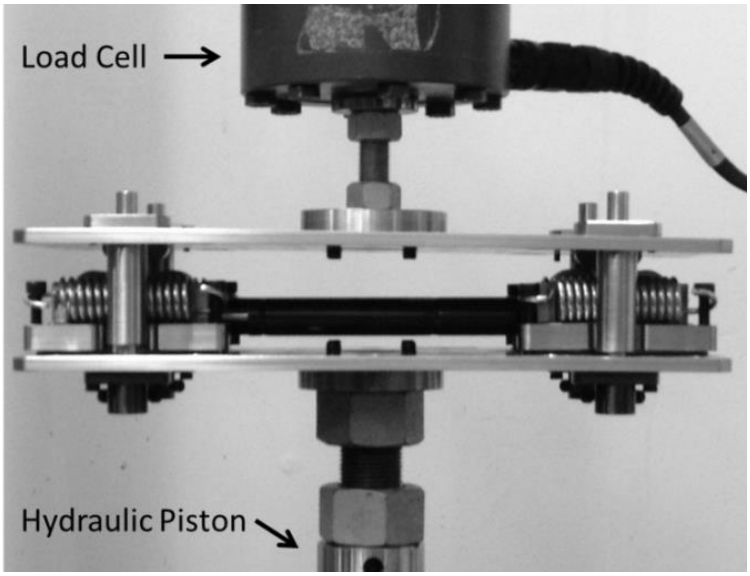

Fig. 10 Single layer prototype in MTS machine

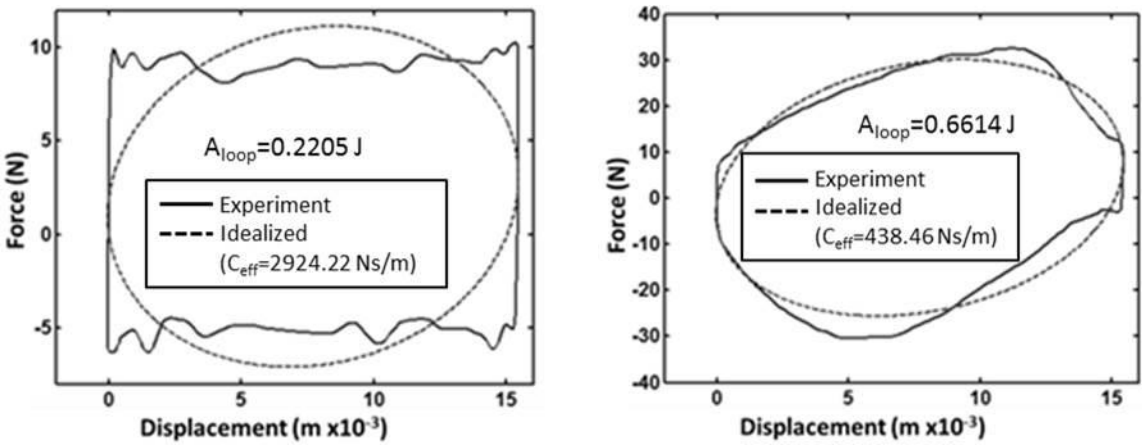

(a) (b)

Fig. 11 Dashpot characterization results at (a) 0.1 Hz, and (b) 2 Hz

N/m springs. Using the measured force, experimental hysteresis loops were plotted and compared with Simscape predictions.

Even before testing the single layer prototype (in Fig. 10), the dashpot alone was characterized. The force versus displacement hysteresis loops for the dashpot are shown in Figs. 11(a) and 11(b) at frequencies of 0.1 Hz, and 2 Hz, respectively. The solid line represents the measured data while the dotted line represents the "idealized" linear hysteresis loops after filtering out all the higher harmonic content in the force response. As indicated in the Analysis section, the idealized loop areas (and energy dissipation) is the same as those of the experimental loops (Gandhi and Wolons 1999). From the idealized loops, the equivalent viscous damping coefficient of the dashpot can be extracted (Lazan 1969) using

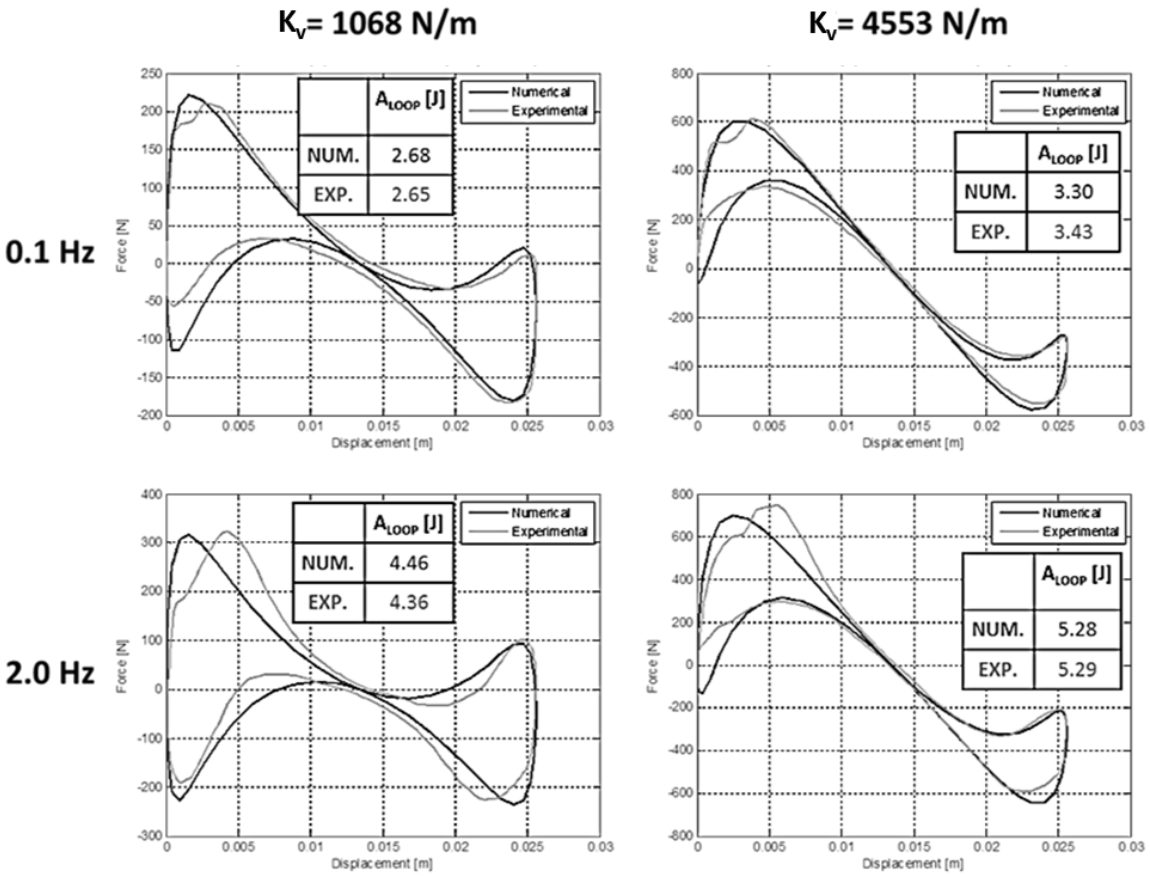

Fig. 12 Hysteresis behavior of single layer prototype under harmonic displacement input

$$C_{eff} = \frac{A_{loop}}{\pi \omega {x_0}^2} \tag{6}$$

where x_0 is half the peak displacement of the system and ω is harmonic excitation frequency.

At low frequency, the effect of friction appears to dominate (Fig. 11(a)), while at higher frequency, the viscosity effects are seen to be more pronounced (Fig. 11(b)). It should be noted that the equivalent viscous damping constant, C_{eff}, is dependent on frequency. The values of C_{eff}, as a function of frequency, obtained from these tests are used in the Simscape simulation results for the single and two layer prototypes.

Experimental and Simscape results for the single layer prototype under harmonic displacement input are presented in Fig. 12. Under displacement control, the hysteresis loops too show the negative stiffness region seen in the static force versus displacement curves in Fig. 2(b) between the stable equilibrium states. It is interesting to note that all of the hysteresis loops are pinched in the central region because the dashpot velocity is very low as it reverses direction. The Simscape simulation results correlate very well with the experimental results both in terms of the shape of hysteresis loops as well as the loop areas. It is observed that at both 0.1 and 2 Hz frequencies, the hysteresis loop area (the energy dissipated) increases with spring stiffness and for both values of

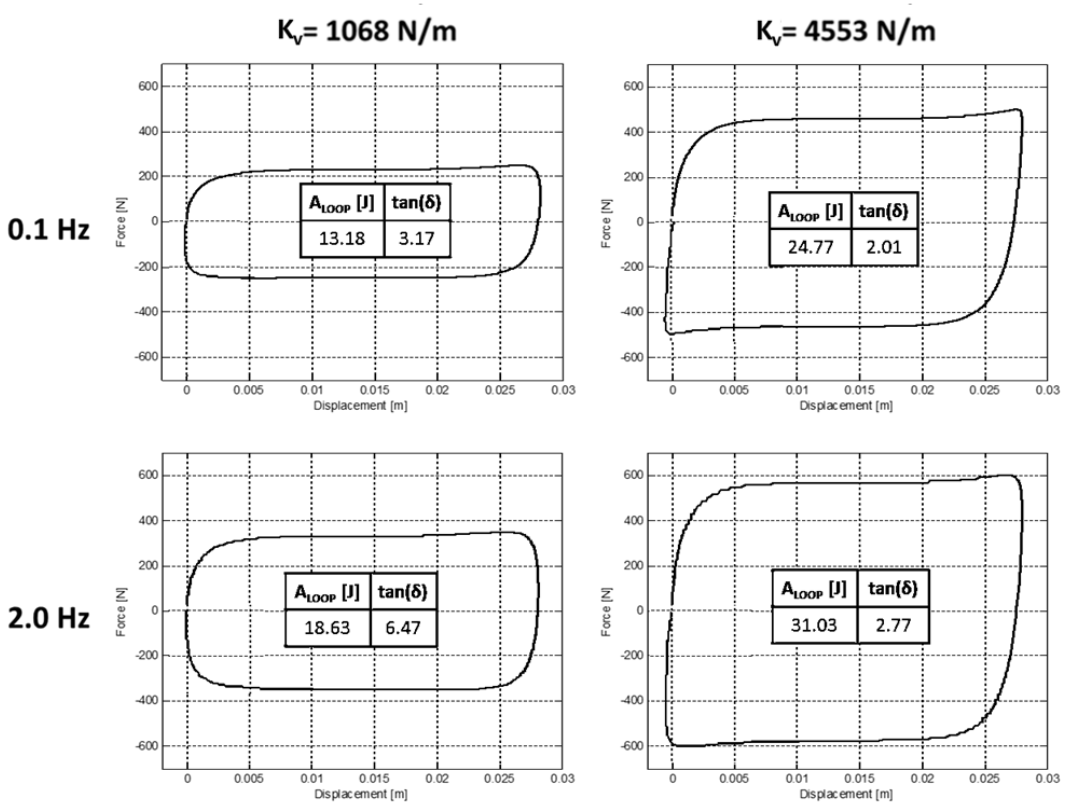

Fig. 13 Simscape predictions of hysteresis behavior of single layer prototype under harmonic force input

VMT spring stiffness, loops area increases with frequency.

For comparison, Simscape results under harmonic force input are presented in Fig. 13. The plateaus in the hysteresis loops are representative of the snap-through behavior expected under force excitation. The trends of increasing hysteresis loop area with increasing frequency and increasing VMT spring stiffness, seen in Fig. 12, are on display here, as well. However, the loop areas and energy dissipation is substantially higher than observed under harmonic displacement inputs (Fig. 12). Also presented on the figures are values of the loss factor, tan δ, indicative of the ratio of energy dissipated to energy stored. Generally, the values of tan δ are very high, indicative of a highly "lossy" system. The higher loss factor values for the lower VMT spring can be attributed to a lower effective stiffness (storage modulus). Under harmonic force input, the stiffer VMT spring leads to a higher effective storage modulus which reduces tan δ even though the energy dissipated (A_{loop}) is actually greater. In summary, the results show that the prototype performs well under harmonic force disturbance over a forcing frequency variation of more than a decade.

7. Two-layer prototype results

The next set of tests was conducted on the two layer prototype with the softer 1,068 N/m VMT

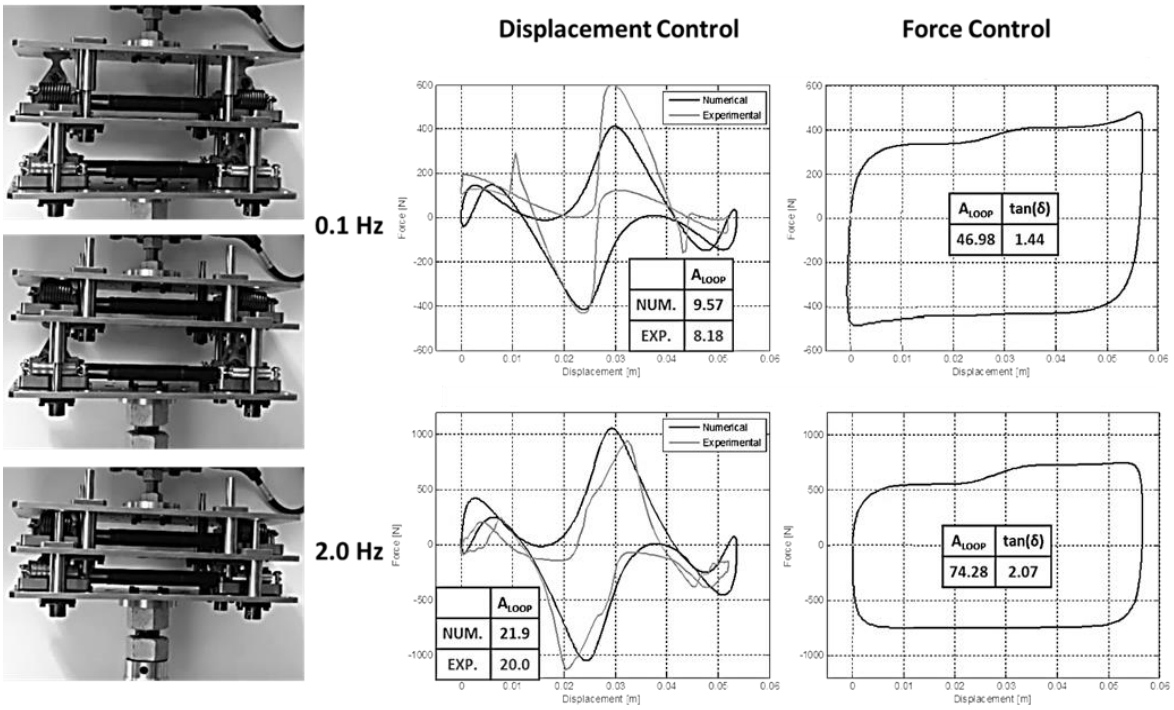

Fig. 14 Two layer prototype under harmonic displacement and load input

springs in the top layer and the stiffer 4,553 N/m VMT springs in the bottom layer. The pictures in the left-most column in Fig. 14 illustrate, in sequence, both layers expanded, followed by the softer top layer compressing first at intermediate load, and finally the stiffer bottom layer compressed, as well, at higher load. The middle column in Fig. 14 shows hysteresis loops under harmonic displacement input at frequencies of 0.1 Hz and 2 Hz. From the displacement axes on the plots it is seen that the stroke is doubled compared to the single layer prototype (Fig. 12). As a result, the hysteresis loop areas have increased. The hysteresis loop shape also shows distinct peaks followed by reduction in force corresponding to the yielding of each of the two layers The Simscape predictions show reasonable agreement with the experimental loops. The right-most column shows Simscape predictions of hysteresis loops under harmonic force input. As was the case with the one layer prototype, the hysteresis loop areas are substantially greater than those obtained under harmonic displacement input.

8. Results for two-layer prototype with pre-loaded springs (PLSs)

To provide significant static load carrying capability to the two layer prototype, four PLSs each having a stiffness of 6,200 N/m were added to each layer. Recall that the pre-compression load in each spring is 254.2 N, so the design static load is 254.2×4=1,017 N. Once this load is exceeded the springs can deform further and the layers can compress. Fig. 15 shows the result of a static compression test of the prototype with the VMT springs in each of the layers removed. Beyond a static load of around 1,000 N, the stiffness in each layer is 6,200 N/m×4 springs=24,800 N/m, and

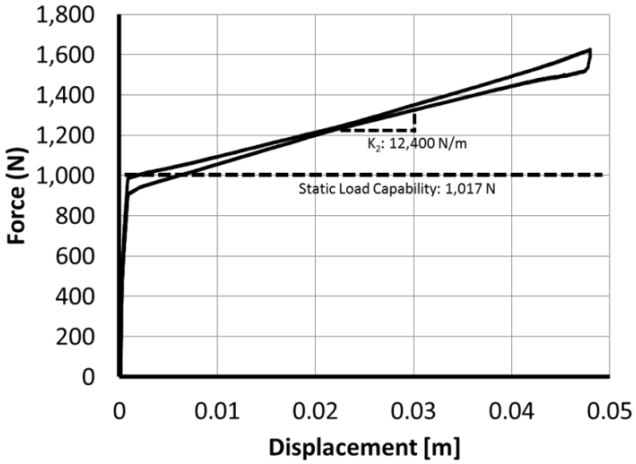

Fig. 15 Static compression test results on two layer prototype with PLSs (VMT springs removed)

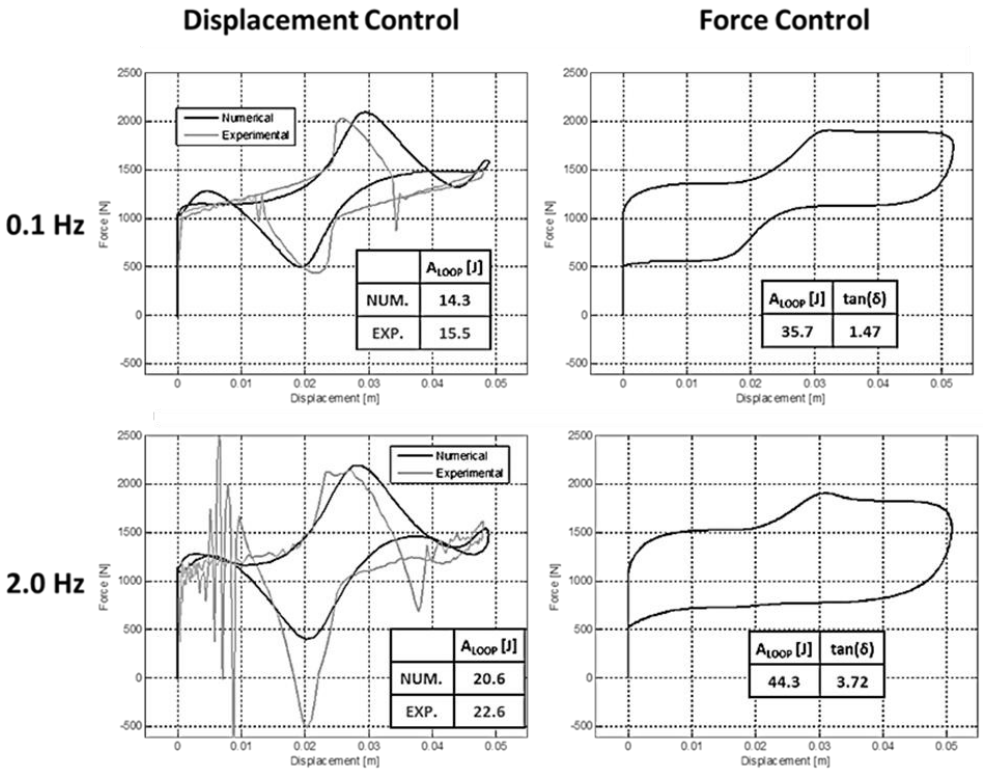

Fig. 16 Experimental and simulation results for the two layer prototype with PLSs under harmonic excitation

considering the two layers in series results in a net secondary stiffness (K_2) of 12,400 N/m.

After introducing the VMT springs into the two layers, the force versus displacement behavior under harmonic displacement input and harmonic force input, at frequencies of 0.1 Hz and 2 Hz, is shown in Fig. 16. The VMT spring stiffness in the soft upper layer is the same as the previous

Table 2 Measured loss factor and energy dissipated per cycle for the prototype compared with a Kelvin-Voigt system

	2 Layer Prototype (w/o PLS)		2 Layer Prototype (w PLS)		Kelvin-Voigt System	
	Displ. Input	Force Input	Displ. Input	Force Input	Displ. Input	Force Input
Loss Factor (0.1 Hz)	-	1.44	-	1.47	0.096	0.096
Loss Factor (2 Hz)	-	2.07	-	3.72	0.285	0.285
Energy Dissipated (*J*) Per Cycle (0.1 Hz)	8.18	46.98	15.50	35.70	10.72	5.35
Energy Dissipated (*J*) Per Cycle (2 Hz)	20.00	74.28	22.60	44.30	32.13	32.52

section (1,068 N/m), but the VMT spring stiffness in the stiff lower layer is increased from 4,553 N/m in the previous section to 14,010 N/m (now thirteen times stiffer than the VMT springs in the soft upper layer). Compared to the results in Fig. 14 (without PLSs) the hysteresis loops are shifted upward on the force axis by an amount corresponding to the pre-compression load (or the design static load). In addition, the secondary stiffness observed in Fig. 15 after the design static load is exceeded, results in a counter-clockwise rotation of the hysteresis loops under harmonic displacement input (although this does not adversely affect energy dissipation capability). Under harmonic displacement input, the correlation between experiment and the Simscape simulation results is acceptable, in general, except the large spikes in force in the experiment due to metal-on-metal contact and exacerbated by the increased stored energy in the PLSs. Compared to Fig. 14, a larger difference between the first and second peaks (under harmonic displacement input) and the first and second plateaus (under harmonic force input) is seen due to the larger difference between the VMT spring stiffnesses in the two layers.

In the 0.1 Hz hysteresis cycle under harmonic force excitation, the difference between plateaus corresponding to the snap-through of the softer VMT layer is observed to be 250 N (implying that snap-through behavior and energy dissipation would be observed at low harmonic force amplitudes of 125 N). The difference between the plateaus corresponding to snap-through of the stiffer VMT layers is observed to be 1325 N (implying good energy dissipation even at much higher harmonic force amplitudes). The ratio of 5.3 between the two indicates that the two layer prototype with the parameters used would be effective in energy dissipation even when the harmonic force amplitude varies by a factor of five.

9. Comparison of the prototype with a Kelvin-Voigt system

The performance of the prototype in Sections 7 and 8 is summarized in terms of loss factor and energy dissipated per cycle in the first four columns of Table 2. This section compares its performance to a reference Kelvin-Voigt system which can be used to represent a typical viscoelastic material or combinations of linear springs and dashpots. Fig. 17 shows a sketch of the reference system comprising of four vertically-oriented dashpots in parallel with four springs, sandwiched between two rigid horizontal plates. The springs each have a constant stiffness, K_{kv}, of 3,100 N/m, which give the system a total stiffness equal to the secondary stiffness of the two-layer prototype with PLSs. The dashpots in the Kelvin-Voigt system are modeled as linear viscous dampers with the same damping coefficient as those used in the prototype (C_{eff}=2924.22 Ns/m at

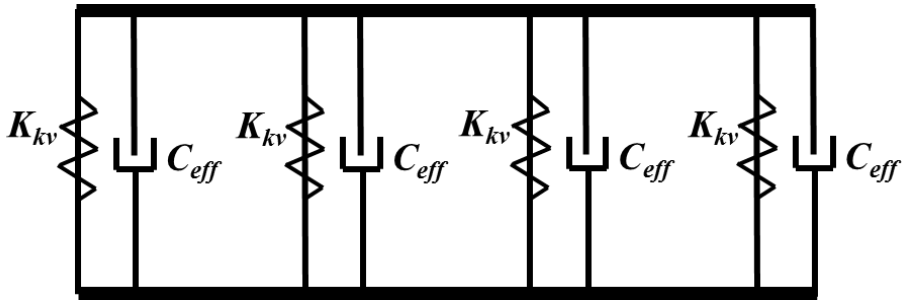

Fig. 17 Kelvin-Voigt viscoelastic system containing four springs of stiffness K_{kv} and four dashpots each with an effective damping constant of C_{eff}

0.1 Hz, or C_{eff}=438.46 Ns/m at 2 Hz). The simulated loss factor and energy dissipated per cycle of the Kelvin-Voigt reference system are tabulated in the 5th and 6th columns of Table 2.

Under displacement input, the loop area of the Kelvin-Voigt model is obtained by rearranging Eq. (6), where x_0 is taken as the total stroke of the two-layer prototype, and loss factor is calculated using Eq. (7).

$$\tan\delta = \frac{C_{eff}\omega}{K_{kv}} \tag{7}$$

To simulate force input, a forcing function described by Eq. (8) is applied, where F_0 is the peak amplitude of the harmonic force applied to the prototype. The differential equation is then solved to obtain the steady state displacement response of the system, given by Eq. (9). As discussed in Section 3, these equations describe a hysteresis loop from which loss factor and hysteresis loop area can be measured.

$$F = F_0\cos(\omega t) = 4C_{eff}\frac{dx}{dt} + 4K_{kv}x \tag{8}$$

$$x = \frac{F_0}{16{K_{kv}}^2 + 16(C_{eff}\omega)^2}\left(4K_{kv}\cos(\omega t) + 4C_{eff}\omega\sin(\omega t)\right) \tag{9}$$

The results in Table 2 for displacement input show that at 0.1 Hz, the Kelvin-Voigt system is comparable to the two layer prototype with or without PLSs, and at 2 Hz the Kelvin-Voigt system dissipates up to 60% more energy per cycle than the prototype. However, it is under force input that the merits of the structural element developed in the present paper become evident. At 0.1 Hz, the structural element with PLSs dissipates over 570% more energy per cycle than the Kelvin-Voigt system, and at 2 Hz it still outperforms the Kelvin-Voigt system by 36-128%. The loss factors of the prototype (calculated under harmonic force input) are also significantly higher than those of the Kelvin-Voigt model over the range of frequencies.

10. Final design modifications for adaptability to one decade in harmonic load amplitude

The results of the prior sections showing good energy dissipation at 0.1 Hz and at 2 Hz demonstrate the effectiveness of the design over a decade of frequency variation. In the last paragraph of Section 8, it was also noted that the prototype demonstrated effectiveness over a

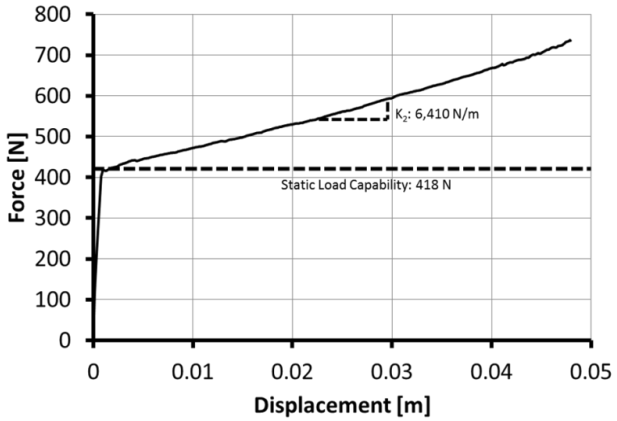

Fig. 18 Static compression test results on the two layer prototype with softer PLSs (VMT springs removed)

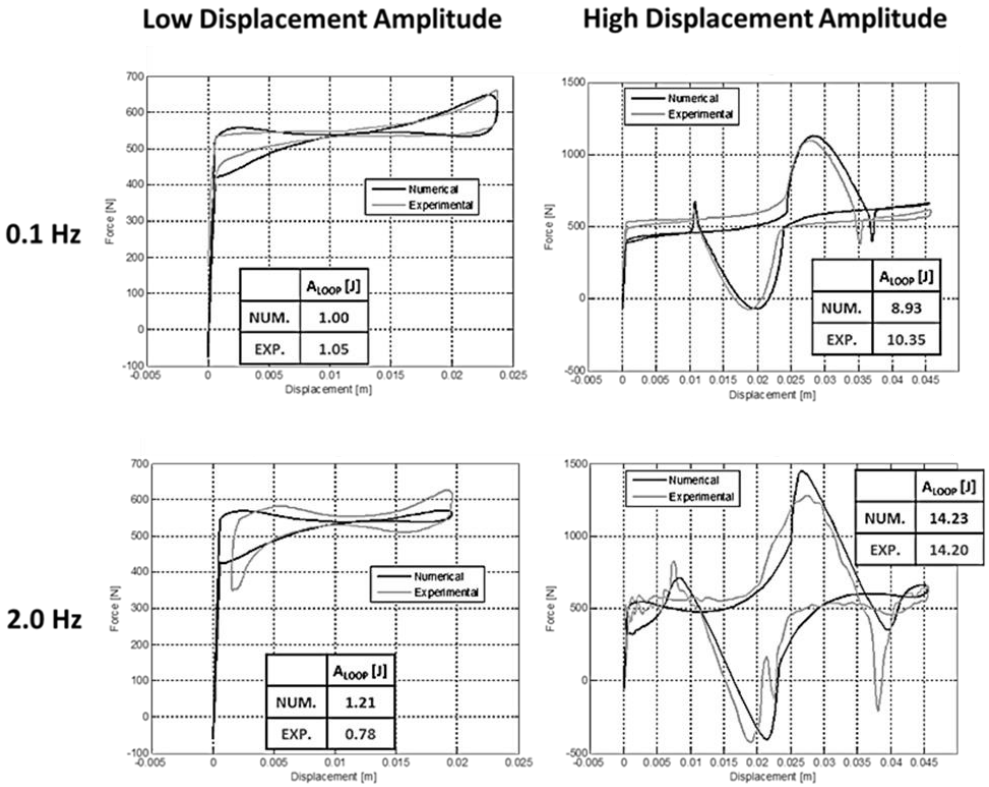

Fig. 19 Experimental and simulation results for the modified (final) two layer prototype with PLSs under harmonic excitation

variation in load amplitude by a factor of five. In this section, a couple of design changes are made so the effectiveness increases to extend over a decade of load amplitude variation. First, the 14,010 N/m stiff VMT spring in the lower layer was replaced by an even stiffer 20,380 N/m spring, further increasing the difference between the snap-through loads of the two layers.

Second, the 6,200 N/m PLSs shown in Fig. 9 and used in the last section were replaced by softer 3,080 N/m PLSs. Although this reduces the static load capability (measured at 418 N in Fig. 18) the reduced secondary stiffness (measured at 6,410 N/m) reduces the peak load associated with the compression of the softer VMT layer, and thus increases the amplitude range of effectiveness of the prototype.

The prototype was then subjected to a harmonic displacement input and the measured and simulated hysteresis loops are shown in Fig. 19. The figures in left column correspond to just the softer layer undergoing compression, whereas those in the right column correspond to compression of both layers. At 0.1 Hz (top row) the peak-to-peak variation of the cyclic load is between 50 and 100 N when the single layer compresses, increasing to 1150 N when both layers are compressed. Clearly, the prototype is able to show effectiveness when the load levels vary in excess of a decade. At 2 Hz (bottom row) the peak-to-peak variation of the cyclic load is about 200 N when the single layer compresses, increasing to between 1650 and 1750 N when both layers undergo compression. Although not exactly a decade, effectiveness is demonstrated at variation in load levels by factor of 8.5 to 9.5.

11. Conclusions

A novel sandwiched-plate-like element was designed with the ability to dissipate energy over a decade of harmonic load amplitudes and over a decade of forcing frequencies while simultaneously supporting a static load. The element absorbs energy through a pair of horizontally-oriented dashpots that are driven by a pair of von-Mises trusses as the VMTs cycle between stable equilibrium states. The compact design of the VMTs allow the mechanism to be sandwiched between two plates such that multiple elements can be arranged to form a continuous panel as well as stacked vertically, with different properties in each layer, for improved load-adaptability. While the VMT parameters of a single layer can be optimized to a particular harmonic load amplitude, having two layers with softer and stiffer VMTs allow the system to show good energy dissipation characteristics at different harmonic load amplitude levels. Also introduced in the elements were pre-loaded springs (PLSs) that provide very high initial stiffness and allow the element to carry a design static load even when the VMTs lose their load carrying capability under harmonic disturbance input. The modeling environment Simscape was used to predict the behavior, and the predictions were correlated against experimental data. Based on the test and simulation results presented in the paper the following observations could be made:

1. Hysteresis behavior of a single layer was examined for VMT spring stiffnesses of 1,068 N/m and 4,553 N/m. Simscape simulations showed good agreement with the experiment under harmonic displacement input, and good energy dissipation (significant hysteresis loop area). Simulation showed even greater energy dissipation (large loop area and loss factor as high as 6.47) under harmonic force input.

2. A second layer was added to the prototype (1,068 N/m top-layer VMT stiffness and 4,553 N/m bottom-layer stiffness) and hysteresis loops were again measured and seen to agree reasonably with simulation. It was observed that distinct peaks in the displacement input loops and plateaus in the case of the force input loops corresponded to the snap-through loads for each layer.

3. Pre-loaded springs having a designed static load of 1,017 N and a secondary stiffness of 12,400 N/m were included in the prototype. The PLSs served to shift the experimental and computational hysteresis loops up on the force axis by the static load level, and the secondary

stiffness produced a counter-clockwise tilt in the loops. The prototype demonstrated adaptability to load amplitudes which varied by a factor of five.

4. This factor was further increased to about a decade by increasing the stiffness of the lower-layer VMT springs to 20,380 N/m and decreasing the stiffness of the PLSs to 3,080 N/m.

5. The prototype also consistently demonstrated adaptability to over a decade of variation in excitation frequency.

6. The prototype has higher loss factors and dissipates significantly more energy per cycle than a conventional viscoelastic load-carrying structure under harmonic force input.

Acknowledgements

The authors gratefully acknowledge the sponsorship of these research activities within the Defense Advanced Research Projects Agency sponsored program at NextGen Aeronautics entitled "Structural Logic" (HR0011-10-C-0189). The views expressed are those of the authors and do not reflect the official policy or position of the Department of Defense or the U.S. Government.

References

Avramov, K.V. and Mikhlin, Y.V. (2006), "Snap-through truss as an absorber of forced oscillations", *J. Sound Vib.*, **290**, 705-722.

Barbarino, S., Pontecorvo, M.E. and Gandhi, F.S. (2012), "Energy dissipation of a bi-stable von-Mises truss under harmonic excitation", *Proceedings of the 53rd AIAA/ASME/ASCE/AHS/ASC Structures, Structural Dynamics and Materials Conference*, Honolulu, HI, April.

Blair, K.B., Krousgrill, C.M. and Farris, T.N. (1992), "Nonlinear dynamic response of shallow arches", *Proceedings of the 33rd AIAA/ASME/ASCE/ASC Structures, Structural Dynamic and Material Conference*, April.

Diaconu, C.G., Weaver, P.M. and Mattonni, F. (2007), "Solutions for morphing airfoil sections using bistable laminated composite structures", *AIAA Structures, Structural Dynamics, and Materials Conference*, April.

Gandhi, F.S. and Wolons, D. (1999), "Characterization of the pseudoelastic damping behavior of shape memory alloy wires using complex modulus", *Smart Mater. Struct.*, **8**, 49-56.

Howell, L.L. (2001), *Compliant Mechanisms*, John Wiley & Sons.

Jensen, B.D. and Howell, L.L. (2004), "Bistable configurations of compliant mechanisms modeled using four links and translational joints", *J. Mech. Des.*, **126**(4), 657-666.

Jensen, B.D., Parkinson, M.B., Kurabayashi, K., Howell, L.L. and Baker, M.S. (2001), "Design optimization of a fully-compliant bistable micro-mechanism", Ann Arbor MI, 48109, 2125.

Johnson, T., Gandhi, F.S. and Frecker, M. (2010), "Modeling and experimental validation of a bistable mechanism for chord extension morphing rotors", *Proc. SPIE 7643, Active and Passive Smart Structures and Integrated Systems 2010*, 76432B, doi:10.1117/12.847661.

Kounadis, A.N., Raftoyiannis, J. and Mallis, J. (1989), "Dynamic buckling of an arch model under impact loading", *J. Sound Vib.*, **134**(2), 193-202.

Lazan, B.J. (1969), *Damping of Materials and Members in Structural Mechanics*, 1st Edition, Pergamon, Oxford.

Mises, R. (1923), "Über die stabilitätsprobleme der elastizitätstheorie (About the stability problems of elasticity theory)", *Zeitschrift Angewandte Mathematik und Mechanik*, **3**, 406-462.

Murray, G.J. and Gandhi, F.S. (2011), "The use of damping to mitigate violent snap-through of bistable systems", *Proceedings of the ASME 2011 Conference on Smart Materials, Adaptive Structures &*

Intelligent Systems (SMASIS), Phoenix, Arizona, USA, September.
Padthe, A.K., Chaturvedi, N.A., Bernstein, D.S., Bhat, S.P. and Waas, A.M. (2008) "Feedback stabilization of snap-through buckling in a preloaded two-bar linkage with hysteresis", *Int. J. Nonlin. Mech.*, **43**, 277-291.
Timoshenko, S.P. (1936), *Theory of Elastic Stability*, McGraw-Hill.

AB